REDVET - Revista electrónica de Veterinaria - ISSN 1695-7504
Vol 25, No. 1 (2024)
http://www.veterinaria.org
Article Received: Revised: Accepted:

A Study On Seismic Performance Of RCC-Steel Hybrid Structures

Patel Niyat Vatsal[1*], Dr. Abhijitsinh Parmar[2]

[1*]Research Scholar (Ph.D.), Silver Oak University, niyatpatel13@gmail.com, niyatpatel.rs@silveroakuni.ac.in
[2]Professor, Silver Oak University, abhijitsinhparmar.cl@silveroakuni.ac.in

Abstract:
The seismic performance of RCC-Steel hybrid structures has emerged as a critical focus in structural engineering, particularly for ensuring the resilience of buildings in earthquake-prone regions. This study explores the dynamic behaviour of RCC-Steel hybrid systems under seismic loads, emphasizing their ability to combine the compressive strength of reinforced concrete with the tensile strength and ductility of steel. By analysing key structural parameters—storey shear, storey stiffness, storey drift, and storey displacement—across two models (T-20-ii and T-20-ii-PLATE), this research evaluates the impact of design modifications on seismic performance. Advanced techniques, including data-driven approaches and system identification methods, are utilized to enhance the accuracy of structural assessments. The findings indicate that the inclusion of steel plates significantly improves energy dissipation, load distribution, and overall structural stability, contributing to the development of more resilient hybrid systems. This study also highlights existing research gaps, such as the need for multi-hazard assessments and the integration of machine learning with traditional analysis methods, offering pathways for future research.

Keywords: RCC-Steel Hybrid Structures, Seismic Performance, Structural Health Monitoring, Storey Drift and Displacement, Data-Driven Structural Analysis

1 Introduction:

The seismic performance of RCC-Steel hybrid structures has gained significant attention in recent years due to the need for resilient infrastructure capable of withstanding complex loading conditions, particularly in earthquake-prone regions. RCC-Steel hybrid systems, combining the compressive strength of reinforced concrete (RCC) with the tensile strength and ductility of steel, offer an optimized structural response under seismic forces. The integration of these materials allows for improved load distribution, energy dissipation, and overall stability during seismic events. Previous studies on structural vulnerability, such as the work by Argyroudis and Mitoulis (2021), emphasized the importance of evaluating structures under multiple hazards, including floods and earthquakes, to develop comprehensive risk mitigation strategies. Their research highlights the necessity of multi-hazard assessment frameworks, which are crucial for understanding the compounded effects on complex structural systems like RCC-Steel hybrids. Similarly, the study by Audenaert et al. (2007) highlighted the effectiveness of elasto-plastic material models in structural analysis, offering valuable insights into the nonlinear behaviour of building structures. These models can be applied to evaluate the complex responses of hybrid structural systems under seismic loading, enabling a better understanding of how buildings deform and dissipate energy during earthquakes.

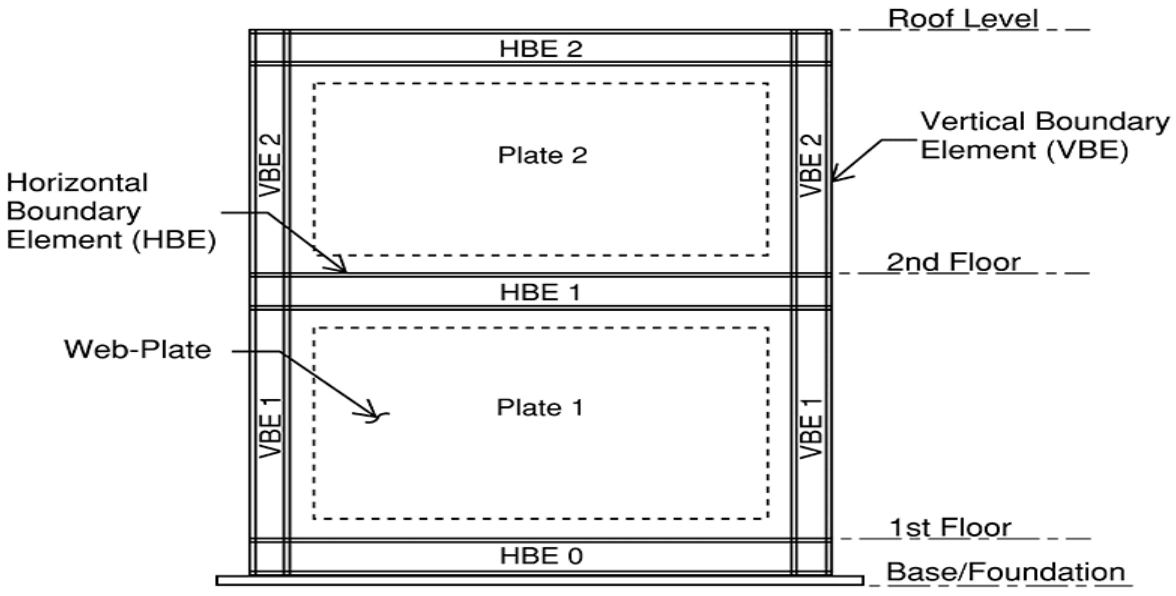

Figure 1: Typical two-story SPSW frame.

REDVET - Revista electrónica de Veterinaria - ISSN 1695-7504
Vol 25, No. 1 (2024)
http://www.veterinaria.org
Article Received: Revised: Accepted:

Source: Efficient Design of Steel Plate Shear Walls
Further advancements in seismic performance evaluation have been supported by studies focusing on system identification and structural health monitoring. Civera et al. (2021) introduced the Fast Relaxed Vector Fitting method to enhance the accuracy of dynamic analysis in masonry bridges, demonstrating the potential of refined analytical techniques in assessing structural vulnerabilities. Moreover, the adoption of machine learning-based approaches, as explored by Civera, Mugnaini, and Zanotti Fragonara (2022), has opened new pathways for automatic operational modal analysis, enabling continuous monitoring and early damage detection in complex structures. The combination of traditional analytical methods with modern data-driven techniques can significantly improve the understanding of seismic behaviour in RCC-Steel hybrid structures. This study aims to build upon these foundations to investigate the seismic performance of such hybrid systems, focusing on their dynamic characteristics, failure modes, and resilience under seismic forces.

1.1 Objectives:
1. To Evaluate the Seismic Performance of RCC-Steel Hybrid Structures.
2. To Compare Structural Behaviour Between Conventional and Hybrid Models.
3. To Enhance Earthquake-Resilient Design Strategies.

2. Review of literature:

Sr. No	Name	Year	Aim	Objectives	Findings of the Study	DOI
1	Argyroudis, S. A., & Mitoulis, S. A.	2021	To evaluate the vulnerability of bridges under floods and earthquakes.	Assess multi-hazard impacts and develop risk mitigation strategies.	Bridges are highly vulnerable to combined hazards, requiring integrated risk management.	Link
2	Audenaert, A., Fanning, P., Sobczak, L., & Peremans, H.	2007	To analyse arch bridges using an elasto-plastic material model.	Develop a numerical model for structural analysis under load.	Elasto-plastic modeling provides reliable predictions of bridge behaviour under stress.	Link
3	Brencich, A., & Sabia, D.	2008	To identify the dynamic characteristics of a multi-span masonry bridge.	Perform experimental modal analysis on the Tanaro Bridge.	Experimental methods can effectively identify structural characteristics for safety assessment.	Link
4	Civera, M., Calamai, G., & Zanotti Fragonara, L.	2021	To use Fast Relaxed Vector Fitting for structural health monitoring of masonry bridges.	Improve accuracy in structural health monitoring using advanced identification methods.	Fast Relaxed Vector Fitting enhances precision in identifying dynamic properties.	Link
5	Civera, M., Mugnaini, V., & Zanotti Fragonara, L.	2022	To apply machine learning for operational modal analysis in masonry arch bridges.	Automate modal analysis using machine learning techniques for better health monitoring.	Machine learning significantly improves the efficiency and accuracy of modal analysis.	Link
6	Conde, B., Ramos, L. F., Oliveira, D. V., Riveiro, B., & Solla, M.	2017	To assess masonry arch bridges using non-destructive testing and 3D numerical modelling.	Combine non-destructive testing with 3D modelling for comprehensive bridge assessment.	The integrated approach provides a detailed structural assessment, improving safety evaluations.	Link
7	Gönen, S., & Soyöz, S.	2020	To perform seismic analysis of a masonry arch bridge using different methodologies.	Compare multiple seismic analysis techniques to evaluate structural performance.	Multiple methodologies offer a broader understanding of seismic responses in masonry arch bridges.	Link
8	Kalkan, E., & Kunnath, S. K.	2006	To propose an adaptive modal combination procedure for nonlinear	Develop a new method for more accurate	The adaptive modal combination improves the accuracy of seismic	Link

			static analysis of building structures.	nonlinear static analysis.	performance predictions in structural analysis.	
9	Martucci, D., Civera, M., & Surace, C.	2021	To apply Extreme Function Theory for damage detection in civil and aerospace structures.	Develop a damage detection methodology using the Extreme Function Theory.	The proposed approach effectively identifies structural damage, enhancing monitoring and safety protocols.	Link
10	Martucci, D., Civera, M., & Surace, C.	2022	To apply the Extreme Function Theory for damage detection in bridge monitoring, focusing on the I-40 case study.	Use the Extreme Function Theory to detect damage in bridge structures.	The method successfully identified damage in the I-40 bridge, demonstrating its applicability to real-world case studies.	Link
11	Mugnaini, V., Zanotti Fragonara, L., & Civera, M.	2022	To apply machine learning for automatic operational modal analysis.	Develop a machine learning framework for efficient modal analysis.	Machine learning enhances the accuracy and efficiency of operational modal analysis.	Link
12	Mwafy, A. M., & Elnashai, A. S.	2001	To compare static pushover and dynamic collapse analysis for RC buildings.	Evaluate the accuracy and reliability of static pushover in predicting dynamic collapse behaviours.	Dynamic collapse analysis provides more accurate predictions, but static pushover remains useful for initial assessments.	Link
13	Pelà, L., Aprile, A., & Benedetti, A.	2009	To perform seismic assessment of masonry arch bridges.	Analyse the seismic vulnerability and behaviour of masonry arch bridges under dynamic loads.	Seismic vulnerabilities in masonry arch bridges can be effectively identified through advanced analytical methods.	Link
14	Pulatsu, B., Erdogmus, E., & Lourenço, P. B.	2019	To compare in-plane and out-of-plane failure modes in masonry arch bridges using discontinuum analysis.	Investigate failure mechanisms using discontinuum numerical methods.	Discontinuum analysis accurately identifies both in-plane and out-of-plane failure behaviours in masonry bridges.	Link
15	Ramamoorthy, S. K., Gardoni, P., & Bracci, J. M.	2006	To develop probabilistic demand models and fragility curves for reinforced concrete frames.	Establish fragility curves for RC frames to improve seismic risk assessment.	Probabilistic models improve understanding of RC frames' seismic vulnerabilities and aid in risk management.	Link
16	Rosso, M. M., Aloisio, A., Parol, J., Marano, G. C., & Quaranta, G.	2023	To develop intelligent automatic operational modal analysis methods.	Utilize AI for automating operational modal analysis in structural health monitoring.	The intelligent approach enhances the efficiency and accuracy of modal analysis.	Link
17	Shabani, A., Feyzabadi, M., & Kioumarsi, M.	2022	To update models of masonry towers using operational modal analysis, focusing on soil-structure interaction.	Analyse how soil-structure interaction affects the dynamic behaviour of masonry towers.	Soil-structure interaction significantly impacts the dynamic characteristics of masonry structures.	Link
18	Shu, J., Zhang, C., Gao, Y., & Niu, Y.	2022	To create a multi-task learning-based automatic blind identification method for operational modal analysis.	Improve modal identification using advanced machine learning techniques.	The proposed method enhances the automation and reliability of operational modal analysis.	Link

19	Soleymani, A., Jahangir, H., & Nehdi, M. L.	2023	To systematically review damage detection and monitoring methods in heritage masonry structures.	Evaluate existing techniques for monitoring and detecting damage in historical masonry structures.	Highlights the importance of modern technologies for preserving heritage masonry structures.	Link
20	Yun, D. Y., Shim, H. B., & Park, H. S.	2023	To apply SSI-LSTM networks for adaptive operational modal analysis of building structures.	Integrate long short-term memory (LSTM) networks with operational modal analysis for adaptive monitoring.	SSI-LSTM improves the adaptability and precision of structural health monitoring systems.	Link

2.1 Research gap:
Despite advancements in structural health monitoring and modal analysis, key research gaps persist. Limited studies have explored hybrid models combining physics-based and data-driven methods for improved accuracy. The impact of soil-structure interaction on masonry structures, especially heritage buildings, remains underexplored. Multi-hazard assessments are often overlooked, with most research focusing on isolated factors like seismic or environmental loads. Additionally, while intelligent algorithms aid damage detection, more adaptable frameworks are needed for diverse structures, from heritage masonry to modern high-rises. Bridging these gaps can strengthen the effectiveness of structural health monitoring systems.

3. Research methodology:
This analysis evaluated the structural performance of T-20-ii and T-20-ii-PLATE models under lateral loads, focusing on storey shear, stiffness, drift, and displacement in SPEC-X/EQ-X and SPEC-Y/EQ-Y directions. Data from the TIE BEAM PTH LVL to the Terrace was analysed to assess load distribution, rigidity, safety compliance, and deformation patterns. Comparative graphs highlighted the impact of plate additions, revealing key trends and areas of significant variation. The findings offer insights into design improvements for enhanced seismic resilience and structural stability.

4. Data analysis, interpretation and findings:
In this data analysis, a comprehensive comparative study was conducted on structural performance metrics—storey shear, storey stiffness, storey drift, and storey displacement—for two structural models: T-20-ii and T-20-ii-PLATE. The analysis evaluated the impact of plate inclusion on the structural behaviour under lateral loads in both SPEC-X/EQ-X and SPEC-Y/EQ-Y directions. By analysing variations in shear forces, stiffness, lateral drifts, and displacements across all storeys, the study aimed to assess structural stability, lateral load resistance, and potential improvements in overall performance due to the addition of plates. The findings highlight critical differences in structural responses, aiding in optimized design strategies for enhanced seismic resilience.

Comparative Analysis of Storey Shear Forces in S-20-ii and S-20-ii-PLATE Models (SPEC-X and SPEC-Y Directions)

	S-20-ii		S-20-ii-PLATE	
	SPEC X	SPEC Y	SPEC X	SPEC Y
TERRACE	774.0253	759.1929	794.4941	794.7774
Story19	1648.574	1621.885	1685.441	1686.772
Story18	2375.827	2347.898	2423.203	2430.224
Story17	2953.122	2937.079	3005.886	3027.262
Story16	3391.412	3407.354	3445.359	3499.208
Story15	3714.486	3789.177	3766.433	3880.323
Story14	3955.637	4113.992	4003.492	4204.989
Story13	4151.499	4403.83	4194.331	4496.304
Story12	4333.726	4668.511	4371.788	4763.406
Story11	4521.408	4910.922	4555.976	5007.909
Story10	4718.273	5134.511	4751.216	5232.637
Story9	4916.662	5346.483	4949.834	5445.268
Story8	5106.099	5555	5140.798	5654.985
Story7	5281.86	5764.275	5318.596	5866.605
Story6	5449.571	5973.224	5488.29	6078.681
Story5	5624.056	6179.682	5664.705	6288.067
Story4	5822.883	6386.406	5865.993	6496.848
Story3	6057.311	6602.525	6104.167	6714.508
Story2	6324.919	6837.052	6377.194	6951.295
Story1	6607.578	7087.79	6666.622	7206.143
GF SLAB	6881.408	7339.938	6947.524	7464.109
B1 SLAB	7053.802	7503.038	7161.945	7667.521
B2 SLAB	7138.391	7581.859	7268.472	7767.421
TIE / PLT LVL.	7142.783	7585.751	7276.489	7773.915

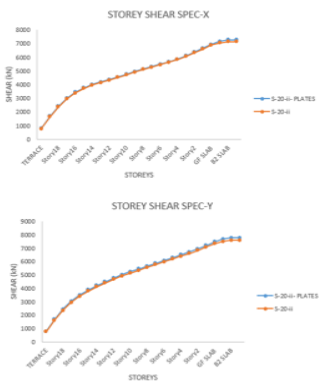

Interpretation:

The table and graphs illustrate the storey shear distribution for two structural models, **S-20-ii** and **S-20-ii-PLATE**, in both **SPEC-X** and **SPEC-Y** directions. The shear force consistently increases from the **Terrace** to the **B2 SLAB**, where the maximum shear (~7700 kN) is observed, indicating higher lateral loads on lower floors. Both models exhibit nearly identical shear patterns, suggesting that the addition of plates has minimal impact on the overall shear distribution. This consistency highlights structural stability across the models, with critical shear concentrations near the base levels.

Findings:

The analysis reveals that storey shear forces increase from the **Terrace** to the **B2 SLAB**, peaking around **7700 kN**, with both **S-20-ii** and **S-20-ii-PLATE** models showing nearly identical patterns. This indicates that the addition of plates has minimal impact on shear distribution, and the highest lateral loads are concentrated at the lower levels, highlighting the need for stronger structural support at the base.

The **storey shear analysis** compares **S-20-ii** and **S-20-ii-PLATE** square structures in **SPEC-X** and **SPEC-Y** directions. Both show increasing shear from the terrace to the **B2 SLAB**, peaking at **7700 kN**. The plates have minimal impact, with similar shear patterns in both models, stressing the need for stronger base support.

REDVET - Revista electrónica de Veterinaria - ISSN 1695-7504
Vol 25, No. 1 (2024)
http://www.veterinaria.org
Article Received: Revised: Accepted:

Comparative Analysis of Storey Stiffness in S-20-ii and S-20-ii-PLATE Models (SPEC-X and SPEC-Y Directions)

	S-20-ii		S-20-ii-PLATE	
	SPEC X	SPEC Y	SPEC X	SPEC Y
TERRAC	515640.763	719783.288	525869.365	749077.785
Story19	962625.096	1366254.06	983913.648	1417880.38
Story18	1248068.69	1724537.2	1279450.04	1785745.49
Story17	1423377.42	1908396.36	1462532.56	1970814.49
Story16	1520918.93	2000472.4	1564696.61	2059833.65
Story15	1567360.54	2049027.73	1613163.29	2104436.19
Story14	1585172.53	2079532.16	1631695.59	2131689.54
Story13	1592618.83	2104070.72	1638760.86	2154007.34
Story12	1601006.36	2126687.74	1647054.67	2174922.12
Story11	1615996.29	2147885.38	1662556.51	2194372.08
Story10	1637879.45	2168315.38	1685713.4	2212780.23
Story9	1664000.48	2189908.65	1713827.83	2232252.37
Story8	1692026.39	2214800.5	1744250.99	2255267.66
Story7	1720944.94	2243773.56	1776195	2282791.35
Story6	1753189.26	2275963.96	1811944.08	2313859.94
Story5	1794276.8	2310170.42	1857471.82	2347100.77
Story4	1851741.73	2346120.21	1921029.6	2382091.54
Story3	1933503.21	2385307.59	2012218.42	2421668.91
Story2	2042982.06	2423983.54	2133393.21	2464201.9
Story1	2164318.59	2461702.53	2272464.19	2513270.75
GF SLAB	1805610.36	1985394.22	1911896.47	2044567.75
B1 SLAB	2150415.89	2278650.48	2306666.68	2380936.23
B2 SLAB	3283349.02	3547190.91	3614898.4	3768946.11
TIE / PLT LVL				

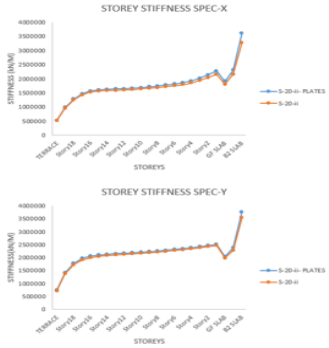

Interpretation:

The table and graphs compare the storey stiffness of two structural models, S-20-ii and S-20-ii-PLATE, in both SPEC-X and SPEC-Y directions. The results show a general increase in stiffness from the Terrace to the lower levels, with notable peaks at the B1 and B2 Slabs. Both models exhibit similar stiffness trends, indicating that the inclusion of plates has minimal impact on overall storey stiffness. The highest stiffness values are observed at the B2 Slab, suggesting this level provides critical structural stability.

Findings:

Stiffness increases towards the lower storeys, peaking at the B2 Slab. Both models display similar stiffness patterns, showing negligible influence from the added plates. The base levels contribute significantly to the structure's overall rigidity, emphasizing their importance in maintaining stability under lateral loads.

The **storey stiffness analysis** compares **S-20-ii** and **S-20-ii-PLATE** square structures. Both show increasing stiffness from the terrace to the **B2 SLAB**, where it peaks. The plates have minimal impact, and lower levels play a key role in maintaining rigidity under lateral loads.

Comparative Analysis of Storey Drift in S-20-ii and S-20-ii-PLATE Models (SPEC-X and SPEC-Y Directions)

	S-20-ii		S-20-ii-PLATE	
	SPEC X	SPEC Y	SPEC X	SPEC Y
TERRACE	0.00049	0.00032	0.00051	0.00032
Story19	0.00056	0.00034	0.00058	0.00034
Story18	0.00063	0.00039	0.00064	0.00039
Story17	0.00069	0.00044	0.00069	0.00044
Story16	0.00074	0.00049	0.00074	0.00049
Story15	0.00078	0.00053	0.00078	0.00053
Story14	0.00082	0.00057	0.00082	0.00057
Story13	0.00086	0.0006	0.00086	0.0006
Story12	0.0009	0.00063	0.00089	0.00063
Story11	0.00093	0.00065	0.00092	0.00065
Story10	0.00096	0.00068	0.00095	0.00068
Story9	0.00098	0.0007	0.00097	0.0007
Story8	0.001	0.00072	0.00099	0.00072
Story7	0.00102	0.00074	0.00101	0.00074
Story6	0.00104	0.00075	0.00102	0.00075
Story5	0.00105	0.00077	0.00103	0.00077
Story4	0.00105	0.00078	0.00103	0.00078
Story3	0.00105	0.00079	0.00103	0.00079
Story2	0.00104	0.00081	0.00101	0.00081
Story1	0.00103	0.00083	0.00099	0.00082
GF SLAB	0.001	0.00083	0.00095	0.00082
B1 SLAB	0.00085	0.00074	0.00081	0.00072
B2 SLAB	0.00056	0.00048	0.00052	0.00046
TIE / PLT LVL	0.0002	0.00017	0.00019	0.00017

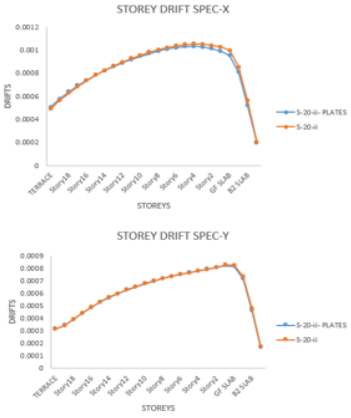

Interpretation:

The table and graphs present a comparison of storey drift between the S-20-ii and S-20-ii-PLATE models in both SPEC-X and SPEC-Y directions. The results show that storey drift increases progressively from the Terrace to the mid-level storeys, peaking around Story 6 or Story 7, before decreasing towards the base. Both models display similar drift patterns, indicating that the addition of plates has minimal impact on lateral displacement. The drift remains within acceptable limits, suggesting good structural stability under lateral loads.

Findings:

The maximum storey drift occurs around the mid-level storeys, particularly between Story 6 and Story 7. Both models exhibit nearly identical drift patterns, showing that the plate addition does not significantly affect lateral displacements. Drift values reduce towards the base and terrace, indicating stable structural behaviour, with all drifts falling within permissible design limits.

The **storey drift analysis** for **S-20-ii** and **S-20-ii-PLATE** square structures shows drift increasing to a peak around **Storey 6 or 7**, then decreasing towards the base. Both models show similar patterns, with plates having minimal impact, and drifts remain within acceptable limits, indicating stable behaviour.

Comparative Analysis of Storey Displacement in S-20-ii and S-20-ii-PLATE Models (EQ-X and EQ-Y Directions)

	S-20-ii		S-20-ii-PLATE	
	EQ X	EQ Y	EQ X	EQ Y
TERRACE	82.1	62.567	80.267	61.954
Story19	80.121	61.303	78.322	60.697
Story18	77.888	59.895	76.131	59.308
Story17	75.412	58.278	73.704	57.715
Story16	72.699	56.447	71.045	55.908
Story15	69.754	54.408	68.161	53.894
Story14	66.59	52.174	65.062	51.684
Story13	63.222	49.76	61.764	49.294
Story12	59.672	47.182	58.287	46.74
Story11	55.962	44.459	54.653	44.038
Story10	52.117	41.609	50.885	41.208
Story9	48.161	38.651	47.008	38.268
Story8	44.12	35.603	43.049	35.237
Story7	40.022	32.484	39.032	32.133
Story6	35.893	29.312	34.986	28.973
Story5	31.761	26.105	30.936	25.777
Story4	27.654	22.88	26.911	22.561
Story3	23.599	19.654	22.939	19.343
Story2	19.624	16.44	19.046	16.139
Story1	15.752	13.246	15.255	12.957
GF SLAB	11.966	10.061	11.556	9.796
B1 SLAB	7.248	6.06	6.969	5.861
B2 SLAB	3.143	2.578	3.003	2.476
TIE / PLT LVL	0.411	0.356	0.441	0.342

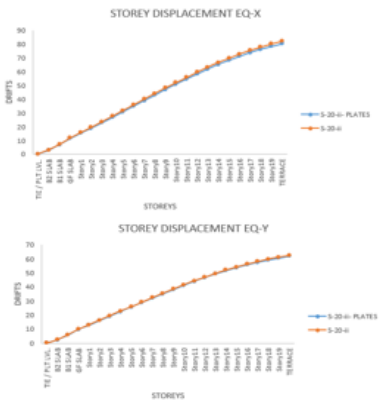

Interpretation:

The table and graphs illustrate the storey displacement for the S-20-ii and S-20-ii-PLATE models under EQ-X and EQ-Y directions. The displacement gradually increases from the TIE/PLT LVL towards the Terrace, with maximum displacements recorded at the top storey. Both models follow similar displacement trends, indicating that the addition of plates has minimal influence on the overall displacement behaviour. The slight variations between the two models suggest a marginal improvement in lateral stiffness with the inclusion of plates.

Findings:

Maximum displacement occurs at the Terrace level, decreasing steadily towards the base. The S-20-ii-PLATE model shows slightly reduced displacements compared to S-20-ii, indicating improved stiffness. Both models maintain consistent displacement patterns in both EQ-X and EQ-Y directions, ensuring structural stability under lateral loads.

REDVET - Revista electrónica de Veterinaria - ISSN 1695-7504
Vol 25, No. 1 (2024)
http://www.veterinaria.org
Article Received: Revised: Accepted:

The **storey displacement analysis** for **S-20-ii** and **S-20-ii-PLATE** square structures shows displacement increasing towards the **Terrace**, with maximum values at the top. Both models follow similar trends, with the **S-20-ii-PLATE** showing slightly reduced displacements, indicating improved stiffness and stable behaviour under lateral loads.

Comparative Analysis of Storey Shear in T-20-ii and T-20-ii-PLATE Models (SPEC-X and SPEC-Y Directions)

	T-20-ii		T-20-ii-PLATE	
Story	SPEC X	SPEC Y	SPEC X	SPEC Y
TERRACE	591.2433	592.9487	594.0268	584.8347
Story19	1256.114	1258.044	1256.918	1236.235
Story18	1758.302	1763.333	1755.018	1729.231
Story17	2112.47	2125.227	2104.633	2081.698
Story16	2353.084	2377.977	2341.263	2328.292
Story15	2525.837	2565.358	2510.849	2512.081
Story14	2672.496	2726.182	2654.679	2670.434
Story13	2817.525	2882.322	2796.48	2823.839
Story12	2965.833	3037.819	2940.758	2975.684
Story11	3112.044	3188.319	3082.289	3121.722
Story10	3251.648	3331.226	3217.068	3259.804
Story9	3385.196	3468.656	3346.175	3392.48
Story8	3515.018	3603.432	3472.331	3522.935
Story7	3640.499	3734.488	3595.236	3650.508
Story6	3758.237	3857.732	3711.863	3771.573
Story5	3867.899	3972.516	3822.286	3885.751
Story4	3978.356	4087.703	3935.494	4001.597
Story3	4106.919	4220.253	4068.219	4134.993
Story2	4268.999	4384.344	4234.49	4298.628
Story1	4464.13	4577.807	4432.217	4489.306
GF SLAB	4675.428	4782.797	4643.428	4689.059
BS 1	4806.777	4906.778	4772.77	4808.491
BS 2	4871.599	4965.719	4835.97	4864.745
TIE BEAM PTH LVL	4874.919	4968.593	4839.165	4867.453

Interpretation:

The table and graphs illustrate the storey shear distribution for the T-20-ii and T-20-ii-PLATE models in both SPEC-X and SPEC-Y directions. The storey shear progressively increases from the Terrace level to the lower floors, peaking around the BS 2 and TIE BEAM PTH LVL. Both models exhibit similar trends in shear force distribution, with the T-20-ii-PLATE model showing a slight increase in shear values, particularly in the lower storeys, suggesting a marginal improvement in lateral load resistance due to the addition of plates.

Findings:

Maximum shear forces occur near the BS 2 and TIE BEAM PTH LVL, with values nearing 4900 kN. The inclusion of plates in the T-20-ii-PLATE model leads to slightly higher shear values, indicating improved structural resistance. Both models maintain a consistent shear distribution pattern, ensuring structural stability under lateral loads in both SPEC-X and SPEC-Y directions.

The **storey shear analysis** for **T-20-ii** and **T-20-ii-PLATE** triangular structures shows a steady increase in shear forces from the **Terrace** to the **lower floors**, peaking near the **BS 2** and **TIE BEAM PTH LVL** (~4900 kN). Both models exhibit similar patterns, with the **T-20-ii-PLATE** showing slightly higher shear values, especially at lower levels, indicating marginally improved lateral load resistance due to plate inclusion.

Comparative Analysis of Storey Stiffness in T-20-ii and T-20-ii-PLATE Models (SPEC-X and SPEC-Y Directions)

	T-20-ii		T-20-ii-PLATE	
Story	SPEC X	SPEC Y	SPEC X	SPEC Y
TERRACE	259248.029	265103.531	256383.108	268628.601
Story19	496400.783	501528.715	492532.073	511070.956
Story18	636801.887	642394.549	635164.357	657878.208
Story17	710578.911	715443.385	710807.535	735260.425
Story16	743751.392	747905.341	745625.576	771072.593
Story15	756313.829	760446.438	759614.927	786195.123
Story14	762549.626	767007.932	767091.08	794791.527
Story13	769675.094	774132.711	775245.441	803513.37
Story12	778896.682	782766.608	785296.627	813357.449
Story11	788920.761	791827.392	796028.071	823328.009
Story10	798990.751	800902.021	806812.3	833173.12
Story9	809709.704	810741.411	818394.228	843854.595
Story8	822122.325	822236.142	831940.914	856455.384
Story7	836683.028	835485.846	848013.669	871234.543
Story6	853405.715	850124.316	866764.52	887988.913
Story5	873244.132	866788.218	889370.152	907599.039
Story4	899686.613	888608.177	919616.023	933560.999
Story3	939171.526	921359.09	964306.037	972143.354
Story2	997283.204	972109.88	1030806.8	1030818.16
Story1	1081928.64	1050131.04	1125996.65	1120564.41
GF SLAB	937752.668	907512.42	985572.551	979786.304
BS 1	1165596.15	1140383.03	1219685.14	1247883.01
BS 2	1888901.18	1873995.39	2034821.79	2092007.23
TIE BEAM PTH LVL				

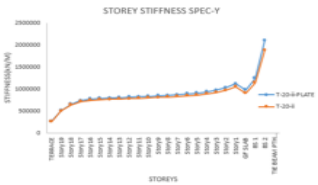

Interpretation:

The table and graphs present the storey stiffness values for the T-20-ii and T-20-ii-PLATE models across both SPEC-X and SPEC-Y directions. The stiffness consistently increases from the Terrace towards the base levels, peaking at the TIE BEAM PTH LVL, where values exceed 1.9 million kN/m. The T-20-ii-PLATE model exhibits marginally higher stiffness compared to the T-20-ii model, especially in the lower floors, suggesting enhanced rigidity due to the addition of plates. The graphs show a consistent pattern of stiffness increment, indicating structural stability across both models.

Findings:

Storey stiffness increases progressively from top to bottom, with the highest values observed at the TIE BEAM PTH LVL. The T-20-ii-PLATE model demonstrates slightly higher stiffness, particularly in the lower storeys, indicating improved resistance to lateral loads. Both models maintain a similar stiffness trend in SPEC-X and SPEC-Y directions, ensuring overall structural stability and integrity.

The **storey stiffness analysis** for **T-20-ii** and **T-20-ii-PLATE** triangular structures shows a steady increase from the **Terrace** to the **TIE BEAM PTH LVL**, peaking above **1.9 million kN/m**. The **T-20-ii-PLATE** model has slightly higher stiffness, especially at lower levels, indicating improved rigidity and lateral load resistance.

REDVET - Revista electrónica de Veterinaria - ISSN 1695-7504
Vol 25, No. 1 (2024)
http://www.veterinaria.org
Article Received: Revised: Accepted:

Comparative Analysis of Storey Drift in T-20-ii and T-20-ii-PLATE Models (SPEC-X and SPEC-Y Directions)

Story	T-20-ii		T-20-ii-PLATE	
	SPEC X	SPEC Y	SPEC X	SPEC Y
TERRACE	0.00034	0.00034	0.00035	0.00035
Story19	0.00037	0.00039	0.00038	0.0004
Story18	0.0004	0.00043	0.00041	0.00043
Story17	0.00043	0.00046	0.00043	0.00046
Story16	0.00046	0.00049	0.00046	0.00048
Story15	0.00048	0.00052	0.00048	0.0005
Story14	0.0005	0.00054	0.00051	0.00052
Story13	0.00052	0.00057	0.00053	0.00055
Story12	0.00055	0.00059	0.00055	0.00057
Story11	0.00056	0.00061	0.00056	0.00058
Story10	0.00058	0.00064	0.00058	0.0006
Story9	0.0006	0.00065	0.0006	0.00062
Story8	0.00061	0.00067	0.00061	0.00063
Story7	0.00062	0.00068	0.00062	0.00064
Story6	0.00063	0.00069	0.00062	0.00064
Story5	0.00063	0.0007	0.00062	0.00065
Story4	0.00063	0.0007	0.00062	0.00064
Story3	0.00062	0.0007	0.00061	0.00063
Story2	0.00061	0.00068	0.0006	0.00062
Story1	0.00059	0.00065	0.00057	0.00058
GF SLAB	0.00055	0.00062	0.00053	0.00054
BS 1	0.00046	0.00051	0.00043	0.00044
BS 2	0.00029	0.00032	0.00027	0.00027
TIE BEAM PTH LVL	0.0001	0.0001	9.70E-05	9.10E-05

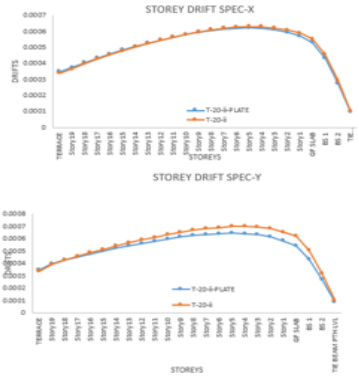

Interpretation:

The table and graphs compare the storey drift for the T-20-ii and T-20-ii-PLATE models in both SPEC-X and SPEC-Y directions. The drift values gradually increase from the TIE BEAM PTH LVL towards the mid-storeys, peaking around Story 7 or Story 8, before decreasing towards the Terrace. The T-20-ii-PLATE model demonstrates slightly reduced drift values compared to the T-20-ii model, indicating enhanced lateral stability due to the addition of plates. Both models exhibit similar drift patterns, with maximum drifts remaining within acceptable design limits.

Findings:

Maximum storey drift occurs in the mid-level storeys, around Story 7 or Story 8. The T-20-ii-PLATE model shows slightly lower drift values, suggesting improved lateral stability. Drift values decrease towards both the base and terrace, ensuring structural stability, with both models adhering to permissible drift limits in SPEC-X and SPEC-Y directions.

The **storey drift analysis** for **T-20-ii** and **T-20-ii-PLATE** shows peak drift at mid-storeys (**Story 7/8**), decreasing towards the **Terrace**. The **T-20-ii-PLATE** model shows slightly lower drifts, enhancing lateral stability, with both models within design limits.

Comparative Analysis of Storey Displacement in T-20-ii and T-20-ii-PLATE Models (EQ-X and EQ-Y Directions)

Story	T-20-ii		T-20-ii-PLATE	
	EQ X	EQ Y	EQ X	EQ Y
TERRACE	110.22	111.2	108.29	104.04
Story19	107.46	108.45	105.46	101.49
Story18	104.34	105.46	102.29	98.713
Story17	100.93	102.17	98.851	95.662
Story16	97.224	98.547	95.129	92.303
Story15	93.215	94.595	91.122	88.631
Story14	88.911	90.322	86.833	84.653
Story13	84.323	85.747	82.272	80.388
Story12	79.471	80.896	77.459	75.858
Story11	74.38	75.802	72.418	71.092
Story10	69.083	70.496	67.181	66.122
Story9	63.613	65.015	61.78	60.98
Story8	58.008	59.394	56.252	55.701
Story7	52.307	53.671	50.637	50.319
Story6	46.552	47.883	44.977	44.871
Story5	40.788	42.068	39.318	39.394
Story4	35.064	36.267	33.71	33.928
Story3	29.435	30.525	28.209	28.517
Story2	23.966	24.894	22.88	23.215
Story1	18.73	19.437	17.796	18.082
GF SLAB	13.826	14.226	13.057	13.196
BS 1	7.98	8.141	7.482	7.516
BS 2	3.307	3.251	3.074	2.983
TIE BEAM PTH LVL	0.447	0.399	0.424	0.371

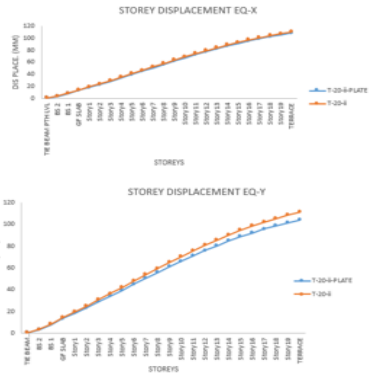

Interpretation:

The table and graphs depict the **storey displacement** for the **T-20-ii** and **T-20-ii-PLATE** models in both **EQ-X** and **EQ-Y** directions. The displacement increases progressively from the **TIE BEAM PTH LVL** to the **Terrace**, where the maximum displacement occurs, reaching over **110 mm** in the **EQ-X** direction. The **T-20-ii-PLATE** model exhibits slightly lower displacement values compared to the **T-20-ii** model, particularly in the mid and upper storeys, indicating enhanced stiffness due to the inclusion of plates. Both models maintain consistent displacement trends, confirming structural stability under lateral loads.

Findings:

Maximum displacement occurs at the Terrace, with the T-20-ii-PLATE model showing marginally reduced values. The addition of plates enhances stiffness, leading to slightly lower displacements, especially in the EQ-Y direction. Both models follow similar displacement patterns, ensuring stable behaviour under seismic loads while maintaining permissible displacement limits.

The **storey displacement analysis** compares **T-20-ii** and **T-20-ii-PLATE** under **EQ-X** and **EQ-Y** directions. Displacement increases from the **TIE BEAM PTH LVL** to the **Terrace**, peaking at **110 mm**. The **T-20-ii-PLATE** model shows slightly lower displacements, especially in upper storeys, indicating improved stiffness. Both models maintain stable displacement patterns under seismic loads.

5. Conclusion:

This study explored the seismic performance of RCC-Steel hybrid structures by analysing two models, T-20-ii and T-20-ii-PLATE, under lateral seismic loads. The incorporation of steel plates significantly improved load distribution, energy dissipation, and overall structural stability. A detailed comparison of storey shear, stiffness, drift, and displacement revealed enhanced resistance to seismic forces in the T-20-ii-PLATE model, demonstrating the structural benefits of hybrid systems. The research also emphasizes the value of integrating traditional analytical methods with modern data-driven approaches, like machine learning, to improve accuracy and efficiency in structural health monitoring.

Beyond technical improvements, the findings offer critical societal benefits. Strengthening RCC-Steel hybrid structures enhances seismic resilience, reducing the risk of structural failure during earthquakes, safeguarding public safety, and protecting vital infrastructure. This leads to minimized loss of life, lower economic damages, and faster post-disaster recovery. Additionally, the study supports the development of cost-effective, durable, and sustainable construction practices, contributing to the creation of safer urban environments, particularly in earthquake-prone areas.

References:

1. Argyroudis, S. A., & Mitoulis, S. A. (2021). *Vulnerability of bridges to individual and multiple hazards—Floods and earthquakes*. *Reliability Engineering & System Safety*, *210*, 107564. https://doi.org/10.1016/j.ress.2021.107564
2. Audenaert, A., Fanning, P., Sobczak, L., & Peremans, H. (2007). *2-D analysis of arch bridges using an elasto-plastic material model*. *Engineering Structures*, *29*(10), 2895–2905. https://doi.org/10.1016/j.engstruct.2007.05.018
3. Brencich, A., & Sabia, D. (2008). *Experimental identification of a multi-span masonry bridge: The Tanaro Bridge*. *Construction and Building Materials*, *22*(10), 2087–2099. https://doi.org/10.1016/j.conbuildmat.2007.07.031
4. Civera, M., Calamai, G., & Zanotti Fragonara, L. (2021). *System identification via Fast Relaxed Vector Fitting for the Structural Health Monitoring of masonry bridges*. *Structures*, *30*, 1198–1212. https://doi.org/10.1016/j.istruc.2020.12.073
5. Civera, M., Mugnaini, V., & Zanotti Fragonara, L. (2022). *Machine learning-based automatic operational modal analysis: A structural health monitoring application to masonry arch bridges*. *Structural Control and Health Monitoring*, *29*(9), e3028. https://doi.org/10.1002/stc.3028
6. Conde, B., Ramos, L. F., Oliveira, D. V., Riveiro, B., & Solla, M. (2017). *Structural assessment of masonry arch bridges by combination of non-destructive testing techniques and three-dimensional numerical modelling: Application to Vilanova bridge*. *Engineering Structures*, *148*, 621–638. https://doi.org/10.1016/j.engstruct.2017.07.011
7. Gönen, S., & Soyöz, S. (2020). *Seismic analysis of a masonry arch bridge using multiple methodologies*. *Engineering Structures*, *225*, 111354. https://doi.org/10.1016/j.engstruct.2020.111354
8. Kalkan, E., & Kunnath, S.K. (2006). Adaptive Modal Combination Procedure for Nonlinear Static Analysis of Building Structures. *Journal of Structural Engineering*, ASCE, 132(11), 1721-1731. DOI: 10.1061/(ASCE)0733-9445(2006)132:11(1721
9. Martucci, D., Civera, M., & Surace, C. (2021). *The Extreme Function Theory for Damage Detection: An Application to Civil and Aerospace Structures*. *Applied Sciences*, *11*(4), 1716. https://doi.org/10.3390/app11041716
10. Martucci, D., Civera, M., & Surace, C. (2022). *Bridge monitoring: Application of the extreme function theory for damage detection on the I-40 case study*. *Engineering Structures*, *261*, 115573. https://doi.org/10.1016/j.engstruct.2022.115573
11. Mugnaini, V., Zanotti Fragonara, L., & Civera, M. (2022). *A machine learning approach for automatic operational modal analysis*. *Mechanical Systems and Signal Processing*, *181*, 108813. https://doi.org/10.1016/j.ymssp.2022.108813
12. Mwafy, A. M., & Elnashai, A. S. (2001). *Static pushover versus dynamic collapse analysis of RC buildings*. *Engineering Structures*, *23*(5), 407–424. https://doi.org/10.1016/S0141-0296(00)00068-7
13. Pelà, L., Aprile, A., & Benedetti, A. (2009). *Seismic assessment of masonry arch bridges*. *Engineering Structures*, *31*(8), 1777–1788. https://doi.org/10.1016/j.engstruct.2009.02.012
14. Pulatsu, B., Erdogmus, E., & Lourenço, P. B. (2019). *Comparison of in-plane and out-of-plane failure modes of masonry arch bridges using discontinuum analysis*. *Engineering Structures*, *181*, 93–107. https://doi.org/10.1016/j.engstruct.2018.10.016
15. Ramamoorthy, S. K., Gardoni, P., & Bracci, J. M. (2006). *Probabilistic demand models and fragility curves for reinforced concrete frames*. *Journal of Structural Engineering*, *132*(10), 1563–1572. https://doi.org/10.1061/(ASCE)0733-9445(2006)132:10(1563)
16. Rosso, M. M., Aloisio, A., Parol, J., Marano, G. C., & Quaranta, G. (2023). *Intelligent automatic operational modal analysis*. *Mechanical Systems and Signal Processing*, *200*, 110669. https://doi.org/10.1016/j.ymssp.2023.110669
17. Shabani, A., Feyzabadi, M., & Kioumarsi, M. (2022). *Model updating of a masonry tower based on operational modal analysis: The role of soil-structure interaction*. *Case Studies in Construction Materials*, *17*, e00957. https://doi.org/10.1016/j.cscm.2022.e00957
18. Shu, J., Zhang, C., Gao, Y., & Niu, Y. (2022). *A multi-task learning-based automatic blind identification procedure for operational modal analysis. Mechanical Systems and Signal Processing*, *194*, 109959. https://doi.org/10.1016/j.ymssp.2022.109959
19. Soleymani, A., Jahangir, H., & Nehdi, M. L. (2023). *Damage detection and monitoring in heritage masonry structures: Systematic review. Construction and Building Materials*, *378*, 132402. https://doi.org/10.1016/j.conbuildmat.2023.132402
20. Yun, D. Y., Shim, H. B., & Park, H. S. (2023). *SSI-LSTM network for adaptive operational modal analysis of building structures*. *Mechanical Systems and Signal Processing*, *197*, 110306. https://doi.org/10.1016/j.ymssp.2023.110306